AIMS Mathematics, 8(2): 4237–4260.
DOI: 10.3934/math.2023211
Received: 25 July 2022
Revised: 13 October 2022
Accepted: 18 October 2022
Published: 02 December 2022

http://www.aimspress.com/journal/Math

Research article

Study of nonlinear thermal convection of ternary nanofluid within Darcy-Brinkman porous structure with time dependent heat source/sink

Kiran Sajjan[1,†], N. Ameer Ahammad[2], C. S. K. Raju[1], M. Karuna Prasad[1], Nehad Ali Shah[3,†] and Thongchai Botmart[4,*]

[1] Department of Mathematics, GITAM School of Science, GITAM Deemed to be University, Bangalore-Campus, Karnataka 562163, India
[2] Department of Mathematics, Faculty of Science, University of Tabuk, P.O. Box741, Tabuk 71491, Saudi Arabia
[3] Department of Mechanical Engineering, Sejong University, Seoul 05006, South Korea
[4] Department of Mathematics, Faculty of Science, Khon Kaen University, Khon Kaen 40002, Thailand

* **Correspondence:** Email: thongbo@kku.ac.th.

[†] These authors contributed equally to this work and are co-first authors.

Abstract: The dynamical behaviour and thermal transportation feature of mixed convective Casson bi-phasic flows of water-based ternary Hybrid nanofluids with different shapes are examined numerically in a Darcy- Brinkman medium bounded by a vertical elongating slender concave-shaped surface. The mathematical framework of the present flow model is developed properly by adopting the single-phase approach, whose solid phase is selected to be metallic or metallic oxide nanoparticles. Besides, the influence of thermal radiation is taken into consideration in the presence of an internal variable heat generation. A set of feasible similarity transformations are applied for the conversion of the governing PDEs into a nonlinear differential structure of coupled ODEs. An advanced differential quadrature algorithm is employed herein to acquire accurate numerical solutions for momentum and energy equations. Results of the conducted parametric study are explained and revealed in graphs using bvp5c in MATLAB to solve the governing system. The solution with three mixture compositions is provided (Type-I and Type-II). Al_2O_3 (Platelet), GNT (Cylindrical), and CNTs (Spherical), Type-II mixture of copper (Cylindrical), silver (Platelet), and copper oxide (Spherical). In comparison to Type-I ternary combination Type-II ternary mixtures is lesser in terms of the temperature distribution. The skin friction coefficient is more in Type-1 compared to Type-2.

Keywords: thermal radiation; Casson rheological model; ternary hybrid nanofluid; porous medium; irregular geometry; local skin friction coefficients
Mathematics Subject Classification: 76–10, 76R10

1. Introduction

Convective heat transfer is one of the most important means of heat exchange in many types of industrial equipment. Several factors influence the convective heat transfer, including device construction, flow patterns, and working fluid characteristics. Traditional working liquids with poor heat conductivity, such as water, oil, ethylene glycol (EG), and lubricants examined by [1,2], significantly limit heat transfer performance. Nanofluids, on the other hand, combine excellent thermal conductivity with lower density to facilitate convective heat transfer in a range of applications. The dynamics of nanofluids owing to thermo-capillary convection generated by distinct five nanoparticle morphologies were given by Jiang et al. [3] (sphere, blade, brick, cylinder, and platelet). The nanofluid created with spherical nanoparticles had the maximum intensity of thermo-capillary convection, whereas platelet-shaped nanoparticles had the lowest. Nusselt numbers increased by 22.8 percent in blade nanoparticles and 2.8 percent in blade-shaped nanoparticles. A comparable work on nanoparticle shape was published by Arno et al. [4] They observed that changing the structure of nanoparticles enhances heat transfer performance, according to Benos et al. [5], Liu et al. [6] studied the significance of quartic autocatalysis on the dynamics of water conveying 47 nm alumina and 29 nm cupric nanoparticles. They presented a comparative analysis between the dynamics of water conveying 29 nm CuO and 47 nm Al_2O_3 on an upper horizontal surface of a paraboloid of revolution. Sabu et al. [7] examined the significance of nanoparticles' shape and thermo-hydrodynamic slip constraints on MHD alumina-water nanoliquid flows over a rotating heated disk with the passive control approach. Several scholars [8,9] have done a great job implementing the MHD paradigm to their study, according to the literature. To examine heat and mass transfer on a stretched sheet, vajravelu [10] utilized suction or blowing. Concentration and temperature distribution were determined using the isothermal moving plate. The temperature distribution in a flow across a stretched sheet with homogeneous heat flux was explored by Dutta, Roy and Gupta [11]. The temperature at a given place drops as the Prandtl number rises. Kumar et al. [12] looked at how MD affected a hybrid nano liquid stream running over an elastic surface. In their study, they concentrated on the influence of the ferromagnetic interaction parameter on flow and temperature sketches. In a 2-dimensional stream of micropolar hybrid nano liquid, Ali et al. [13] used MD to evaluate the impacts of varying volume percentages on involved distributions.

The influence of rotations on the thermal deterioration of a flexible Walters' (model B') elastico-viscous fluids in porous media was explored by Rana and Kango [14] using linearized stability theory. In a Brinkman porous medium, Kuznetsov and Nield [15] examined the thermos dynamic instability of a permeable media surface saturated with a nanofluid. While Sheu [16] investigated the linear stability of convection in a viscoelastic nanofluid surface. Nonlinear stretching sheets are often used by researchers to better model a variety of real-world flow concerns, such as lowering the weightiness and acoustic of complicated mechanical microstructures. The researchers were interested in the boundary layer flows that occurred from linear/nonlinear stretching sheets of varying geometrical thicknesses because of their significant

industrial applications. Lee [17] was the first to offer an effective geometrical boundary layer flow structure, which has since sparked a lot of controversy among scientists. Chen's study focused on mixed convective fluxes across thin bodies [18]. Fang and his colleagues are a set of people who collaborate to solve difficulties [19]. The impact of velocity drops on three-dimensional stretching/shrinking flow was studied by Jusoh et al. [20], Jama'ludin et al. [21], and Khashi'ie et al. [22] using nanofluid. The Boussinesq estimate expresses that while the distinction in inactivity is little, gravity is adequately amazing to make the particular loads of the two liquids vary altogether. The Boussinesq estimate is utilized to tackle issues including liquid stream and warmth move where the temperature of the liquid changes starting with one area then onto the next. Mass, force, and energy are completely saved in the liquid. Varieties in liquid qualities other than thickness are ignored in the Boussinesq estimation, and thickness arises just when it is increased by gravity's velocity increase. Stability analysis was used in these tests to assess the steady flow solution's reliability, further worthwhile the nonlinear buoyancy-induced (quadratic convection) flow of hybrid nanofluid fields are analyzed comprehensively by investigators [23–32] and reported that the hybrid nanoparticles have intermediate kind of conductivity in the flow mechanism.

After, thorough literature collection in present study, considered the nonlinear convective flow in suspended Darcy porous layers and ternary nanoparticles. With appropriate transformation, the resulting ruling partial differential system is changed into a governing ordinary differential system, and a solution with two mixture compositions is supplied (Type-I and Type-II). Type-I mixture of Al_2O_3 (Platelet), GNT (Cylindrical), and CNTs (Spherical), Type-II mixture of silver (Platelet), copper (Cylindrical), and copper oxide (Spherical). The combination of liquids is of great importance in various systems such as medical treatment, manufacturing, experimental instrument design, aerosol particle handling and naval academies, etc. Roseland's quadratic and linear approximation of three-dimensional flow characteristics with the existence of Boussinesq quadratic buoyancy and thermal variation. In addition, we combine tertiary solid nanoparticles with different shapes and densities. In many practical applications such as the plastics manufacturing and polymer industry, the temperature difference is remarkably large, causing the density of the working fluid to vary non-linearly with temperature. Therefore, the nonlinear Boussinesq (NBA) approximation cannot be ignored, since it greatly affects the flow and heat transport characteristics of the working fluid. Here, the flow of non-Newtonian elastomers is controlled by the tension of an elastic sheet subjected to NBA and the quadratic form of the Roseland thermal radiation is studied.

2. Mathematical modelling

The summary and plot are embedded within a Darcy-Brinkman porous structure, where permeability $K(x)$ is a nonlinear function of x.as shown schematically in Figure 1.

A continuous two-dimensional mixed convection of a radiative Casson Hybrid nanofluid is generated via a wedge shaped thin sheet of varying thickness. Indeed, the Viscoelastic Hybrid nanofluid is chemically created by dissolving a volume fraction of metallic/metallic oxide nanoparticles in a volumetric amount of sodium alginate (SA), which rheological follows the Casson fluid model. In a two-dimensional Cartesian frame (x, y), the present Hybrid nanofluid flow arrangement may be visualised geometrically as a thin sheet stretching upwards in a homogeneous gravitational field of strength g, with a variable velocity $u_h(x)$. The varying temperature of the walls Tw warms the stretched sheet unevenly $T_h(x)$.

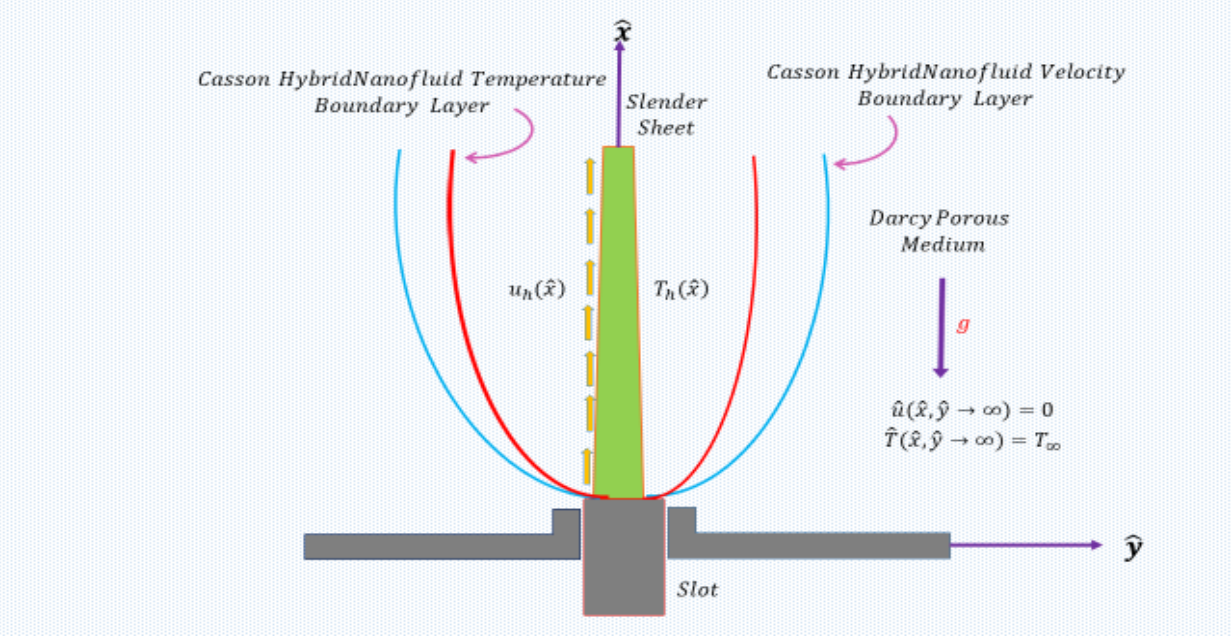

Figure 1. Flow geometry.

The temperature in the free-stream zone is also maintained at T_∞ meaning that the Hybrid nanofluid is at rest. Using boundary layer simplifications, the governing equations for the current flow issue are presented [23] i.e., $v << u, \partial/\partial x << \partial/\partial y, \partial^2/\partial x^2 << \partial^2/\partial y^2$ and the Oberbeck-Boussinesq approximation in its linearized version [24] and Alghamdi et al. [31]:

$$\frac{\partial v}{\partial y}+\frac{\partial u}{\partial x}=0, \tag{1}$$

$$\rho_{hnf}\left(u\frac{\partial u}{\partial x}+v\frac{\partial u}{\partial y}\right)=-\frac{\partial p}{\partial x}+\mu_{hnf}\left(\frac{\beta+1}{\beta}\right)\frac{\partial^2 u}{\partial y^2}-\left(\frac{(\beta+1)\mu_{hnf}}{\beta k_x}\right)u$$
$$-g\left[\rho_{hnf}-(\rho_{\beta T})_{hnf}\{\beta_1(T-T_\infty)^2+\beta_o(T-T_\infty)\}\right], \tag{2}$$

$$\left(\frac{\partial p}{\partial y}\right)=0, \tag{3}$$

$$(\rho c_p)_{hnf}\left(v\frac{\partial T}{\partial y}+u\frac{\partial T}{\partial x}\right)=k_{hnf}\frac{\partial^2 T}{\partial y^2}+\frac{\partial}{\partial y}\left(\frac{16\sigma_e T^3}{3\beta_r}\frac{\partial T}{\partial y}\right)+\frac{k_f u_w(x)}{\gamma_f(x+a)}\left\{\frac{A[T_w-T_\infty]u}{u_w(x)}+B[T-T_\infty]\right\}, \tag{4}$$

$$\frac{\partial p}{\partial x}=-\rho_{hnf}g. \tag{5}$$

With the following dimensions Boundary Conditions:

$$\begin{aligned} &v[x,y=\varepsilon(x)]=0, u[x,y=\varepsilon(x)]=u_h(x),\\ &T[x,y=\varepsilon(x)]=T_h(x),\\ &T[x,y\to\infty]\to T_\infty, u[x,y\to\infty]\to 0. \end{aligned} \tag{6}$$

The radiative heat flow vector $q_r=(q_{rx},q_{ry})$ within optically thick medium may be written as follows [24,29] using the Rosseland approximation [25]:

$$q_r = -\frac{4}{3\beta_R}\nabla(e_b), \tag{7}$$

$$e_b = \sigma_e T^4. \tag{8}$$

Given the previous considerations, the powered temperature T^4 is linearized near the free-stream temperature T_∞ as follows [28]:

$$T^4 = 4T_\infty^3 T - 3T_\infty^4. \tag{9}$$

The following formulas may be used to assess the Hybrid nanofluid thermophysical characteristics provided in the preceding formulation:

$$\left.\begin{aligned} \mu_{hnf} &= \frac{\phi_3\mu_{nf3}+\phi_2\mu_{nf2}+\phi_1\mu_{nf1}}{\phi} \\ k_{hnf} &= \frac{k_{nf1}\phi_1+k_{nf2}\phi_2+k_{nf3}\phi_3}{\phi} \end{aligned}\right\}. \tag{10}$$

We study the viscosity and thermal conductivity of ternary hybrid nanoparticles. To assess the form of the nanoparticles, researchers employed a variety of viscosity and thermal conductivity models for platelet, cylindrical, and spherical nanoparticles. The form of nanoparticles influences their density, therefore this was critical for a correct model. Higher-density nanoparticles contain a nanofluid with changing thermal conductivity and viscosity. The ternary hybrid nanofluid density model is used by Raju et al. [24]:

$$\rho_{hnf} = (1-\phi_3-\phi_2-\phi_1)\rho_{bf} + \phi_3\rho_{sp3} + \phi_2\rho_{sp2} + \phi_1\rho_{sp1}. \tag{11}$$

The heat capacity of a ternary hybrid nanofluid may be calculated using the formula given by Raju et al. [24]:

$$(\rho c_p)_{hnf} = [1-\phi_3-\phi_2-\phi_1](\rho c_p)_{bf} + \phi_3(\rho c_p)_{sp3} + \phi_2(\rho c_p)_{sp2} + \phi_1(\rho c_p)_{sp1}. \tag{12}$$

For spherical nanoparticles, thermal conductivity models and viscosity are applied.

$$\left.\begin{aligned} \frac{\mu_{nf1}}{\mu_{bf}} &= 1 + 2.5\phi + 6.2\phi^2 \\ k_{nf1} &= k_{bf}\left[\frac{k_{sp1}+2k_{bf}-2\phi(k_{bf}-k_{sp1})}{k_{sp1}+2k_{bf}+\phi(k_{bf}-k_{sp1})}\right] \end{aligned}\right\}. \tag{13}$$

For cylindrical nanoparticles, the viscosity and thermal conductivity models are applied (Raju et al. [24]).

$$\left.\begin{aligned} \frac{\mu_{nf2}}{\mu_{bf}} &= 1 + 13.5\phi + 904.4\phi^2 \\ k_{nf2} &= k_{bf}\left[\frac{k_{sp2}+3.9k_{bf}-3.9\phi(k_{bf}-k_{sp2})}{k_{sp2}+3.9k_{bf}+\phi(k_{bf}-k_{sp2})}\right] \end{aligned}\right\}. \tag{14}$$

Platelet nanoparticles have thermal conductivity models and viscosity.

$$\left.\begin{aligned} \frac{\mu_{nf3}}{\mu_{bf}} &= 1 + 37.1\phi + 612.6\phi^2 \\ k_{nf3} &= k_{bf}\left[\frac{k_{sp3}+4.7k_{bf}-4.7\phi(k_{bf}-k_{sp3})}{k_{sp3}+4.7k_{bf}+\phi(k_{bf}-k_{sp3})}\right] \end{aligned}\right\}. \tag{15}$$

The volume of spherical nanoparticles is ϕ_1, cylindrical nanoparticles are ϕ_2, and platelet nanoparticles are ϕ_3. The amount of total volume is expressed as a percentage of the whole volume.

$$\phi = \phi_1 + \phi_2 + \phi_3. \tag{16}$$

It is ideal for ternary hybrid nanofluids with $\phi > 0.02$ value, according to models with varied thermal characteristics (Raju et al. [24]).

$$\left.\begin{aligned}
&A_2 = 1 - \phi_1 - \phi_2 - \phi_3 + \phi_1 \frac{\rho_{sp1}}{\rho_{bf}} + \phi_2 \frac{\rho_{sp2}}{\rho_{bf}} + \phi_3 \frac{\rho_{sp3}}{\rho_{bf}} \\
&B_1 = 1 + 2.5\phi + 6.2\phi^2, B_2 = 1 + 13.5\phi + 904.4\phi^2 \\
&B_3 = 1 + 37.1\phi + 612.6\phi^2, B_4 = \frac{k_{sp1}+2k_{bf}-2\phi(k_{bf}-k_{sp1})}{k_{sp1}+2k_{bf}+\phi(k_{bf}-k_{sp1})} \\
&B_5 = \frac{k_{sp2}+3.9k_{bf}-3.9\phi(k_{bf}-k_{sp2})}{k_{sp2}+3.9k_{bf}+\phi(k_{bf}-k_{sp2})}, B_6 = \frac{k_{sp3}+4.7k_{bf}-4.7\phi(k_{bf}-k_{sp3})}{k_{sp3}+4.7k_{bf}+\phi(k_{bf}-k_{sp3})} \\
&A_1 = B_3\phi_3 + B_2\phi_2 + B_1\phi_1, A_3 = B_6\phi_3 + B_5\phi_2 + B_4\phi_1 \\
&A_4 = 1 - \phi_3 - \phi_2 - \phi_1 + \frac{(\rho c_p)_{sp3}}{(\rho c_p)_{bf}}\phi_3 + \frac{(\rho c_p)_{sp2}}{(\rho c_p)_{bf}}\phi_2 + \phi_1 \frac{(\rho c_p)_{sp1}}{(\rho c_p)_{bf}}
\end{aligned}\right\}, \tag{17}$$

the values of the thermophysical properties of nanoparticles are presented in Table 1.

The given similarity adjustments are included into controlling PDEs to get the dimensionless versions of the boundary layer results:

$$\left.\begin{aligned}
&\xi = x\left(\frac{b}{\upsilon_f}\right)^{(1+n)^{-1}}, u_h(x) = (x+a)^n b \\
&\zeta = \left[\sqrt{\left\{\frac{1}{\{x+a\}^{(1-n)}}\left[\frac{b}{\upsilon_f}\right]\left(\frac{n+1}{2}\right)\right\}}\right] y, \theta(\zeta) = \frac{T-T_\infty}{T_h-T_\infty}, u = \{x+a\}^n b F'(\zeta) \\
&v = -\left[\frac{1}{\{x+a\}^{(1-n)}}\left(\frac{n+1}{2}\right) b\upsilon_f\right]^{\frac{1}{2}}\left[\left(\frac{n-1}{n+1}\right)\zeta F'(\zeta) + F(\zeta)\right]
\end{aligned}\right\}. \tag{18}$$

The following dimensionless ODEs of (Alghamdi et al. [31]):

$$\left(1+\frac{1}{\beta}\right)\frac{\mu_r}{\rho_r} f''' + ff'' - \left(\frac{2n}{n+1}\right) f'^2 - \left(\frac{2}{n+1}\right)\left(1+\frac{1}{\beta}\right)\frac{\mu_r}{\rho_r} P + \left(\frac{2}{n+1}\right)\lambda(1+\theta Q_c)\theta\frac{(\rho_{\beta T})_r}{\rho_r} = 0, \tag{19}$$

$$\left[k_r + R_D\{(\theta_p - 1)\theta + 1\}^3\right]\theta'' + \left(\frac{2}{n+1}\right)[AF' + B\theta] + \theta' F\, Pr(\rho_{cp})_{hnf}$$

$$+\left\{R_D(\theta')^2 3(\theta_p - 1)[\theta(\theta_p - 1) + 1]^2\right\} = 0, \tag{20}$$

where,

$$(\rho\beta_T)_r = \frac{(\rho\beta_T)_{hnf}}{(\rho\beta_T)_f}, \rho_r = \frac{\rho_{hnf}}{\rho_f}, (\rho C_p)_r = \frac{(\rho C_p)_{hnf}}{(\rho C_p)_f}, \mu_r = \frac{\mu_{hnf}}{\mu_f}, k_r = \frac{k_{hnf}}{k_f}, \sigma_r = \frac{\sigma_{hnf}}{\sigma_f}. \tag{21}$$

The dimensionless Boundary conditions that regulate Eqs (19) and (20) are as follows:

$$F(\zeta = \chi) = \left(\frac{1-n}{1+n}\right)\chi, F'(\zeta = \chi) = 1, \theta(\zeta = \chi) = 1, \tag{22}$$

$$F'(\zeta \to \infty) \to 0, \theta(\zeta \to \infty) \to 0. \tag{23}$$

The nomenclature table explicitly defines the included dimensional/dimensionless quantities and variables. The mixed convection phenomenon is controlled by the following variables in this study:

$$\lambda = \frac{Gr_x}{Re_x^2} = \left[\frac{c(\rho\beta_T)g}{b^2\rho_f}\right](x+a)^{(m-2n+1)}. \tag{24}$$

As a result, the linear relationship below should be used to link the temperature and velocity power parameters (*m, n*) in order to find adequate similarity solutions:

$$m = 2n - 1. \tag{25}$$

The following transformations are used to make the succeeding computational tasks easier:

$$\{\zeta = \eta + \chi, F(\zeta) = F(\eta+\chi) = f(\eta), \theta(\zeta) = \theta(\eta+\chi) = \theta(\eta)\}. \tag{26}$$

As a result, the following simplified differential structure emerges:

$$\begin{gathered}
f(\eta=0) = \left(\frac{1-n}{n+1}\right)\chi, \\
f'(\eta=0) = 1, \\
\left(\frac{1}{\beta}+1\right)\frac{\mu_r}{\rho_r}f''' + ff'' - f'^2\left(\frac{2n}{n+1}\right) - \frac{\mu_r}{\rho_r}P\left(\frac{2}{n+1}\right)\left(\frac{1}{\beta}+1\right) + \left(\frac{2}{n+1}\right)\lambda(1+\theta Q_c)\theta\frac{(\rho_{\beta T})_r}{\rho_r} = 0, \\
f'(\eta\to\infty)\to 0, \\
\theta(\eta=0) = 1, \\
\left[k_r + R_D\{(\theta_p-1)\theta+1\}^3\right]\theta'' + \left(\frac{2}{n+1}\right)[AF' + B\theta] + \theta' F\, Pr(\rho_{cp})_{hnf} \\
+\left\{R_D(\theta')^2 3(\theta_p-1)[\theta(\theta_p-1)+1]^2\right\} = 0, \\
\theta(\eta\to\infty)\to 0.
\end{gathered} \tag{27}$$

The xy-shear stress component τ_h and the vertical wall heat flux q_h are the fundamental quantities of concern in the current convective flow at the stretched sheet, and are defined as:

$$\tau_h = \mu_{hnf}\left(1+\frac{1}{\beta}\right)\left(\frac{\partial u}{\partial y} + \frac{\partial v}{\partial x}\right)_{y=\varepsilon(x)}, \tag{28}$$

$$q_h = -\left(k_{hnf} + \frac{16\sigma_e T_\infty^3}{3\beta_R}\right)\left(\frac{\partial T}{\partial y}\right)_{y=\varepsilon(x)}. \tag{29}$$

Those engineering quantities are computed locally in the dimensionless forms as:

$$Nu_r = Re_x^{-\frac{1}{2}} N\, u_{fx} = -\left(\frac{n+1}{2}\right)^{\frac{1}{2}}(k_r + R_D)\theta'(0), \tag{30}$$

$$C_{fr} = -\,Re_x^{\frac{1}{2}} C_{fx} = -(2n+2)^{\frac{1}{2}}\mu_r\left(1+\frac{1}{\beta}\right)f''(0), \tag{31}$$

in which,

$$C_{fx} = \frac{\tau_h}{\frac{1}{2}\rho_f u_h^2(x)}, \tag{32}$$

$$Nu_x = \frac{(x+a)q_h}{k_f(T_h - T_\infty)}, \tag{33}$$

$$Re_x = \frac{(x+a)u_h(x)}{\upsilon_f}. \tag{34}$$

The numbers with no dimensions as previously mentioned, *Nux* and *Cfx* signify the local Nusselt number and wall frictional factor, respectively, whereas *Nur* and *Cfr* denote their reduced equivalents.

Table 1. The thermophysical properties of nanoparticles Elnaqeeb et al. [30]

	Nanoparticle and base fluid naming conventions	*K (W/mk)*	c_p *(1/kgK)*	ρ *(kg/m^3)*	Shapes of Nanoparticle
Hybrid Nanofluid 1	Aluminum oxide Al_2O_3 (0.05%)	40	765	3970	Platelet
	Carbon nanotubes (0.01%)	3007.4	410	2100	Spherical
	Graphene (0.05%))	5000	790	2200	Cylindrical
Hybrid Nanofluid 2	Silver *(Ag)* (0.05%)	429	235	10,500	Platelet
	Copper oxide *CuO (0.01%)*	20	535.6	6500	Spherical
	Copper *(Cu)* (0.05%)	400	385	8933	Cylindrical
Base fluid	Water H_2O	0.623	4.179	997.1	

3. Methodology and authentication

The nonlinear differential equation with the boundary constraints (27) are solved numerically using Runge-Kutta integration method. Initially, the set of nonlinear ODEs converted to 1st order differential equations, by using the following process is given by (Upadhya and Raju [32]).

$$f = y_1, f' = y_2, f'' = y_3, \theta = y_4, \theta' = y_5, \tag{35}$$

$$\left(\frac{1}{\beta}+1\right)\frac{\mu_r}{\rho_r}f''' = f'^2\left(\frac{2n}{n+1}\right) - ff'' + \frac{\mu_r}{\rho_r}P\left(\frac{2}{n+1}\right)\left(\frac{1}{\beta}+1\right) - \left(\frac{2}{n+1}\right)\lambda(1+\theta Q_c)\theta\frac{(\rho_{\beta T})_r}{\rho_r},$$

$$\left[k_r + R_D\{(\theta_p - 1)\theta + 1\}^3\right]\theta'' = -\left(\frac{2}{n+1}\right)[AF' + B\theta] - \theta' F\, Pr(\rho_{cp})_{hnf}$$

$$-\left\{R_D(\theta')^2 3(\theta_p - 1)\left[\theta(\theta_p - 1) + 1\right]^2\right\} = 0, \tag{36}$$

with boundary conditions as:

$$y_1 = \left(\frac{1-n}{n+1}\right)\chi, y_2 = 1, y_2(\eta \to \infty) \to 0, y_4(\eta = 0) = 1, y_4(\eta \to \infty) \to 0. \tag{37}$$

We guess the values of $y_3(0)$ which are not specified at the initial conditions. The Eqs (35)–(37) are integrated by taking the help of Runge-Kutta method with the successive iterative step length as 0.01. For this, used MATLAB bvp5c solver to solve the first order nonlinear coupled differential equations. The correctness of the supposed values is checked by equating the calculated values $y_1(0), y_2(0), y_4(0)$ at $\varsigma = \varsigma_{max}$with their given values at $\varsigma = \varsigma_{max}$. If any difference between their corresponding values

exists, then the process is continued upto the required good values. Alternatively, we are using the Runge-Kutta method to get the accurately found the initial values of $y_1(0), y_2(0), y_4(0)$ and then integrate Eqs (35)–(37). This process is repeated until the settlement between the designed value and the given condition is within the specified degree of accuracy 10^{-5}. In order to validate the precision of the current solutions, compared our results with Khader and Megahed [33] solutions and found earnest agreement with Khader and Megahed [33] solutions under the limited case displayed in Table 2.

Table 2. Validation of the values of friction factor when $n = 0.5,\ B = \phi_3 = R_D = \theta_p = Q_c = \beta = 0,\ M = \phi_1 = \phi_2 = A = 0.$

λ	Khader and Megahed [33]	Current results
0.2	-0.9248	-0.9248
0.25	-0.73339	-0.7333
0.5	-0.75957	-0.7596

4. Interoperation of physical quantities and their discussions

The results indicate how non-dimensional controlling factors affect dimensionless sketches. $f'(\eta), \theta(\eta),\ and\ \eta$ such as radiation parameter (R), Dimensional positive characteristics (n), a nonlinear convection parameter or a quadratic convection parameter (Qc), the ternary hybrid nanofluid's volume fraction (φ), temperature ratio parameter (θ_p), heat source parameters $(A\&B)$, mixed convection parameter (λ), Prandtl number (p_r) (see Figures 2–19). $p_r = 6.7, A = B = 0.01, \lambda = 0.5, \varphi = 0.5, R = 0.5, \theta_p = 0.1, Qc = 0.1, P = 1, and \beta = 2$ are the default parameter values utilised in the simulation. These values were kept constant throughout the research, with the exception of the varied values shown in the relevant figure.

The variation in skin friction coefficients and the Nusselt number as the Dimensional positive features parameter (n) rises the Nusselt number and the friction coefficient is shown in Figure 20(a) for both situations 1 and 2. For both scenarios 1 and 2, the variation in skin friction coefficients and the Nusselt number when the quadratic thermal radiation parameter R enhances the Nusselt number while decreasing the friction coefficient is shown in Figure 20(b). For both Cases 1 and 2, Figure 20(c) depicts the fluctuation in skin friction coefficients and Nusselt number when the volume fraction parameter (ϕ) decreases the Nusselt number and raises the friction coefficient. For both Cases 1 and 2, Figure 20(d) depicts the variation in skin friction coefficients and Nusselt number when the mixed convection parameter (λ) reduces the Nusselt number while increasing the friction coefficient. The variation in the skin friction coefficients and the Nusselt number when the temperature ratio parameter (θ_p) raises the Nusselt number and decreases the friction coefficient is shown in Figure 20(e) for both Cases 1 and 2. For both Cases 1 and 2, Figure 20(f) depicts the variation in skin friction coefficients and Nusselt number when Prandtl number (Pr) decreases the Nusselt number while increasing the friction coefficient. Figure 20(g) shows how the skin friction coefficients and the Nusselt number change when the nonlinear convection parameter (Q_c) lowers the Nusselt number and raises the friction coefficient in both Case 1 and 2. For both Cases 1 and 2, Figure 20(h, i) depicts the variation in skin friction coefficients and the Nusselt number when Heat source characteristics $(A\&B)$ lower the Nusselt number while increasing the friction coefficient. The influence of the Dimensional positive features parameter (n)on temperature and velocity sketches is seen in Figures 2 and 3. It has been shown that as the Dimensional positive features parameter is increased, both velocity sketches and temperature sketches increases. Figures 4 and 5 demonstrate the effect of a quadratic thermal radiation parameter (R)on non-

dimensionless velocities and temperature. The figures show that increasing the quadratic thermal radiation parameter increases both the fluid's temperature and velocity sketches. The influence of the Volume fraction parameter of the ternary hybrid nanofluid (φ) on temperature and velocity sketches is depicted in Figures 6 and 7. The data show that raising the Volume fraction parameter of the ternary hybrid nanofluid lowers the velocity sketches and increases the temperature profiles.

The effect of the mixed convection parameter (λ) on temperature and velocity sketches is seen in Figures 8 and 9. As can be seen, raising the mixed convection value enhances the velocity sketches and decreases the temperature profiles. Figures 10–11 show the effect of the temperature ratio parameter (θ_p) on temperature and velocity sketches. When the temperature ratio parameter is raised, both the temperature and velocity sketches are visibly increased. Figures 12 and 13 show the impact of the Prandtl number (Pr) on temperature and velocity curves. It has been discovered that when the Prandtl number increases, so the temperature and velocity sketches decrease. Figures 14 and 15 depicts the influence of the nonlinear convection parameter (Q_c) on temperature and velocity sketches. It is self-evident that increasing the nonlinear convection parameter raises velocity sketches and decreases the temperature profiles. Figures 16 and 17 depicts the influence of the Heat source factor (A) on temperature and velocity sketches. Increases in the Heat source parameter result in higher velocity and temperature sketches. Figures 18 and 19 show the effect of the Heat source factor (B) on temperature graph. It is obvious that as the Heat source parameter is increased, both temperature and velocity sketches rise.

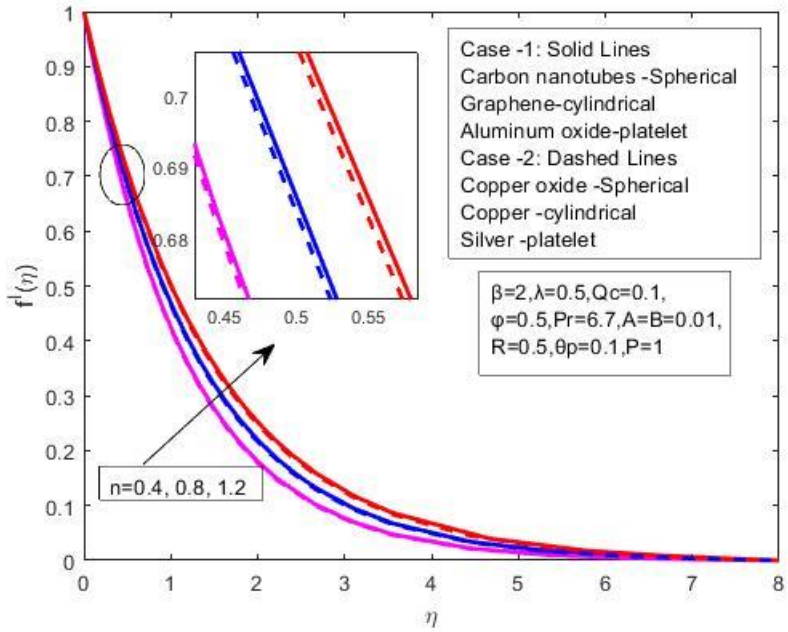

Figure 2. Velocity graphs for various (n) values for two different ternary hybrid nanofluids.

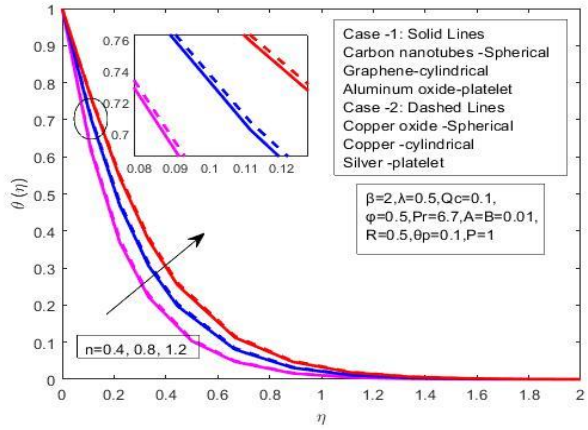

Figure 3. Temperature graphs for various (n) values for two different ternary hybrid nanofluids.

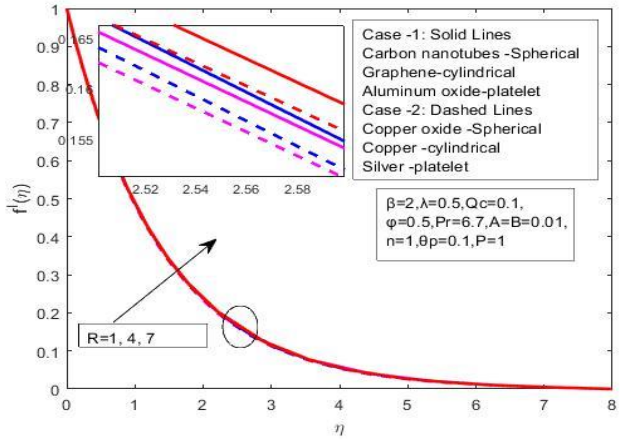

Figure 4. Velocity graphs for various (R) values for two different ternary hybrid nanofluids.

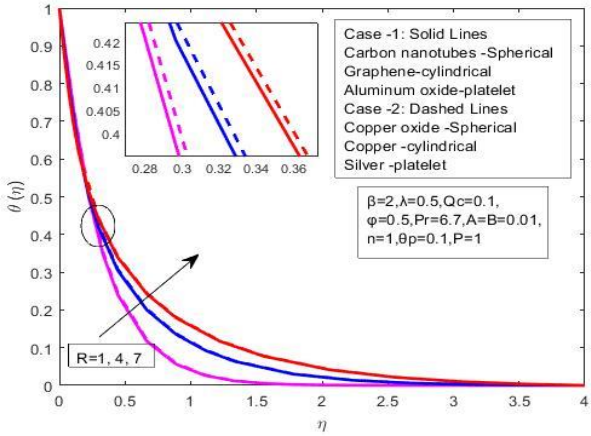

Figure 5. Temperature graphs for various (R) values for two different ternary hybrid nanofluids.

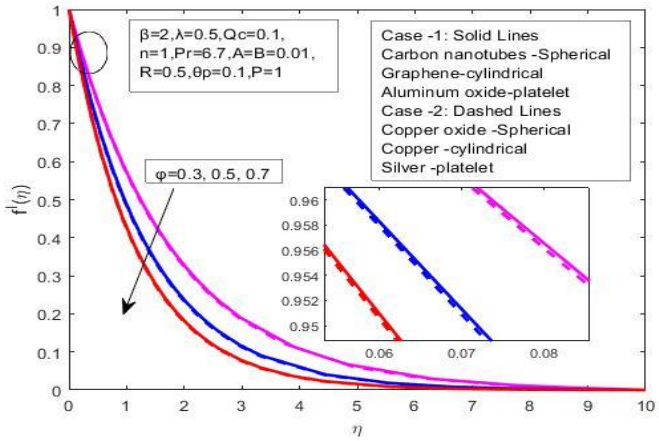

Figure 6. Velocity graphs for various (ϕ) values for two different ternary hybrid nanofluids.

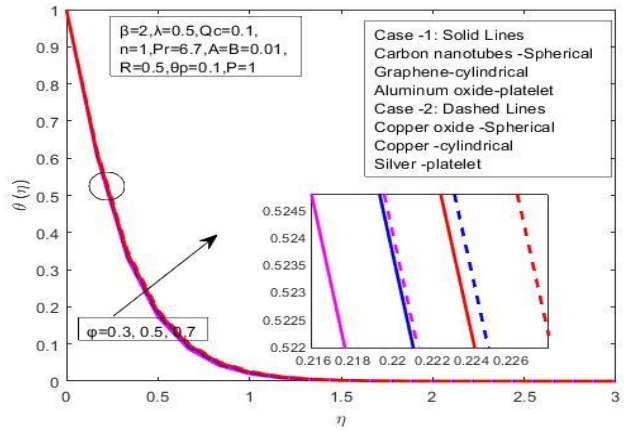

Figure 7. Temperature graphs for various (ϕ) values for two different ternary hybrid nanofluids.

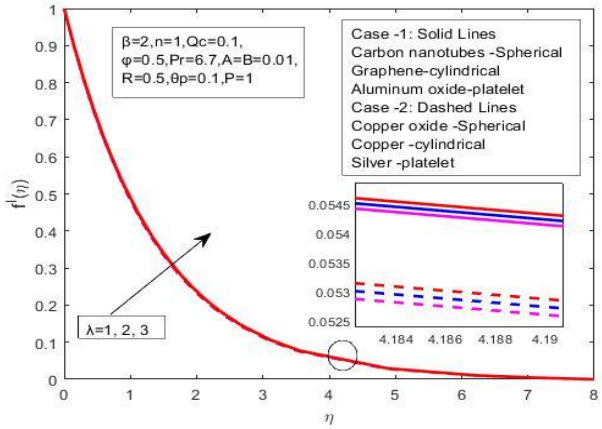

Figure 8. Velocity graphs for various (λ) values for two different ternary hybrid nanofluids.

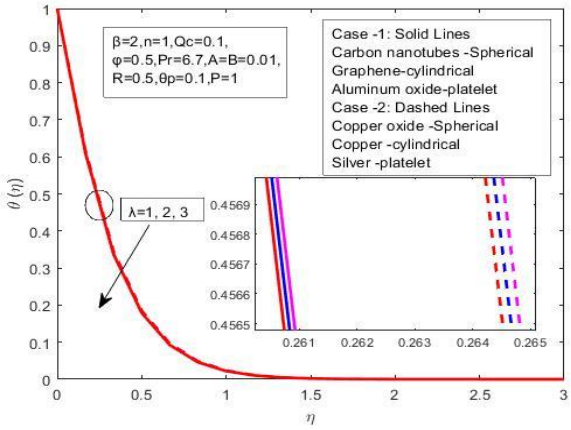

Figure 9. Temperature graphs for various (λ) values for two different ternary hybrid nanofluids.

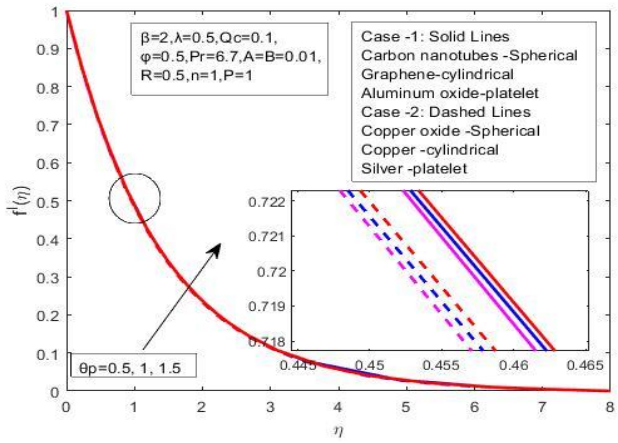

Figure 10. Velocity graphs for various (θ_p) values for two different ternary hybrid nanofluids.

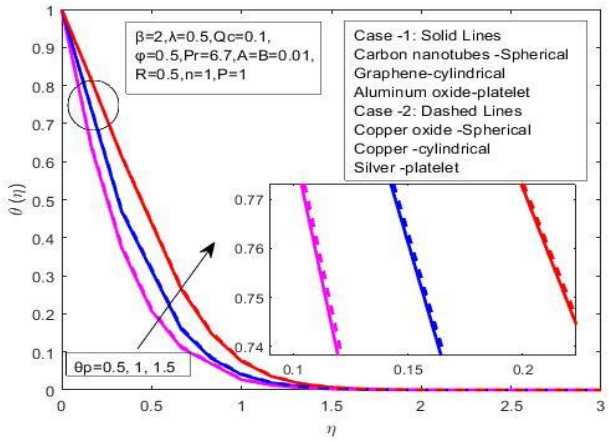

Figure 11. Temperature graphs for various (θ_p) values for two different ternary hybrid nanofluids.

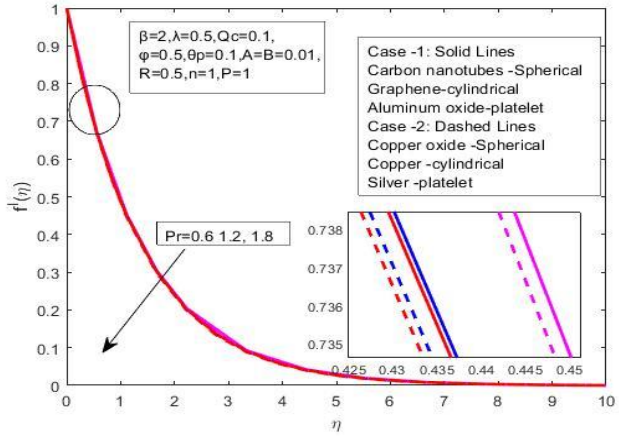

Figure 12. Velocity graphs for various (Pr) values for two different ternary hybrid nanofluids.

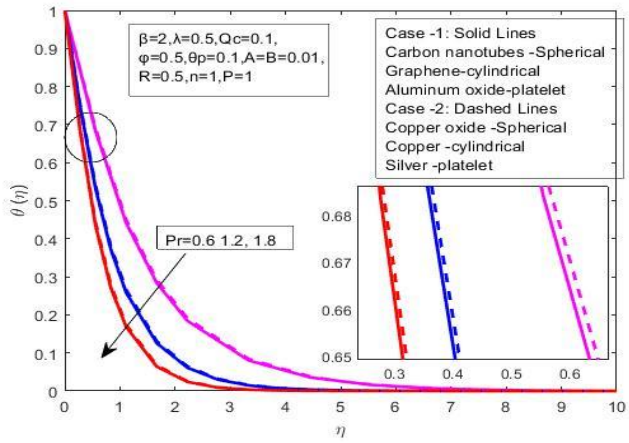

Figure 13. Temperature graphs for various (Pr) values for two different ternary hybrid nanofluids.

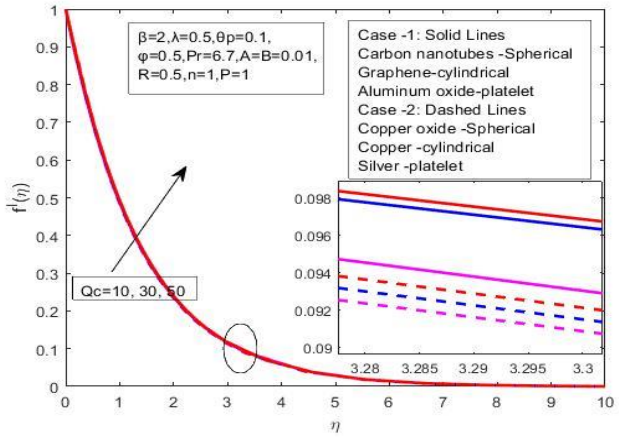

Figure 14. Velocity graphs for various (Q_c) values for two different ternary hybrid nanofluids.

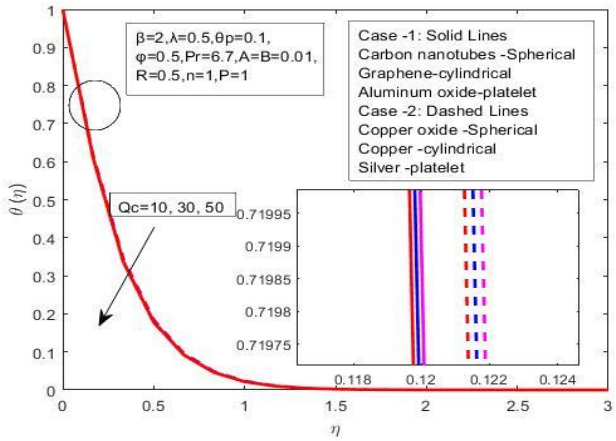

Figure 15. Temperature graphs for various (Q_c) values for two different ternary hybrid nanofluids.

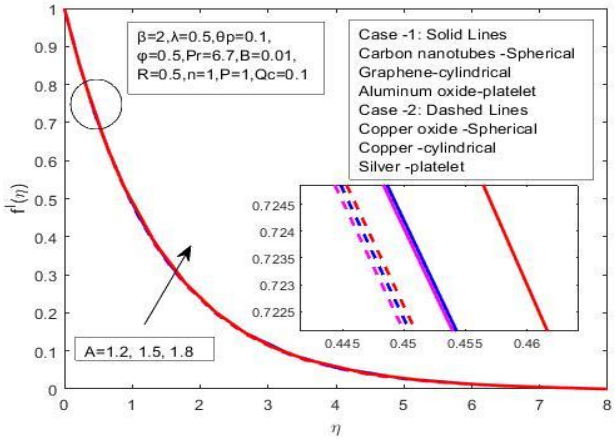

Figure 16. Velocity graphs for various (A) values for two different ternary hybrid nanofluids.

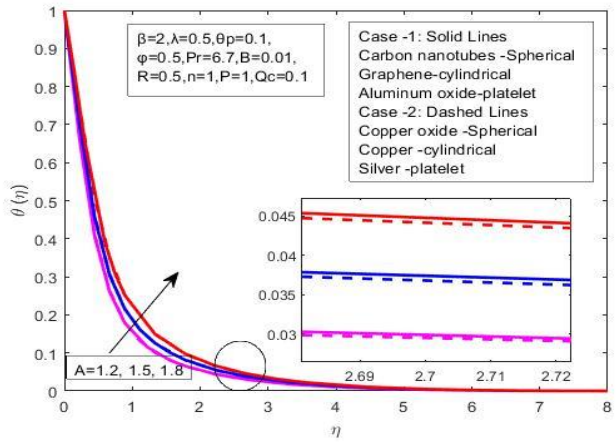

Figure 17. Temperature graphs for various (A) values for two different ternary hybrid nanofluids.

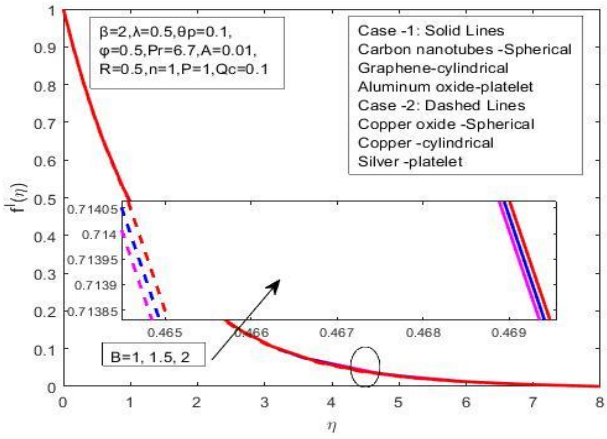

Figure 18. Velocity graphs for various (B) values for two different ternary hybrid nanofluids.

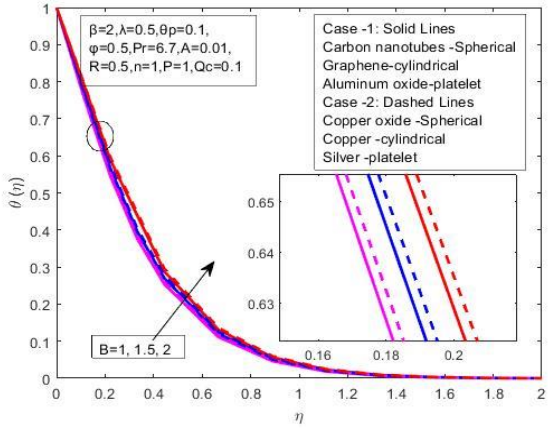

Figure 19. Temperature graphs for various (B) values for two different ternary hybrid nanofluids.

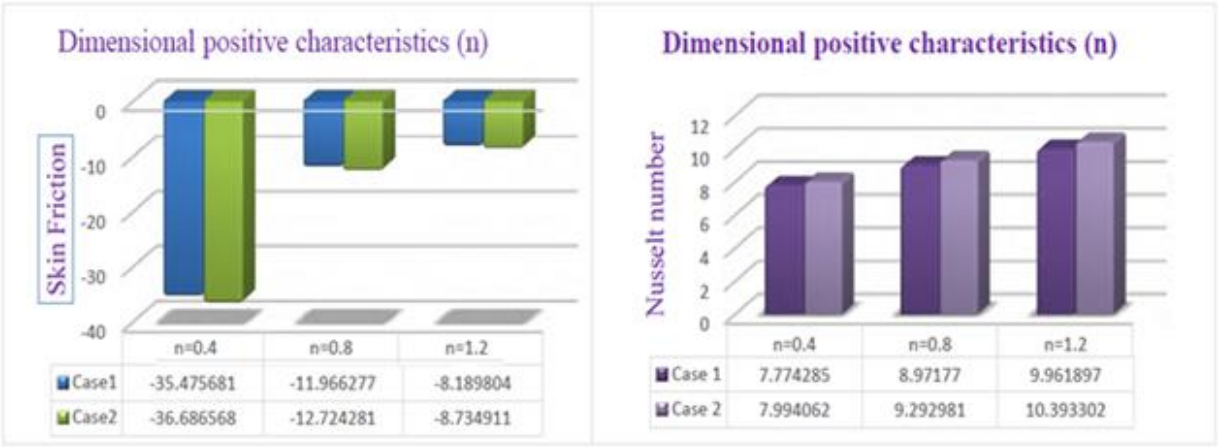

Figure 20(a). Depicts the bar graph of dimensional positive characteristics (n) with Nusselt number and skin friction for two different combination of ternary hybrid nanofluid.

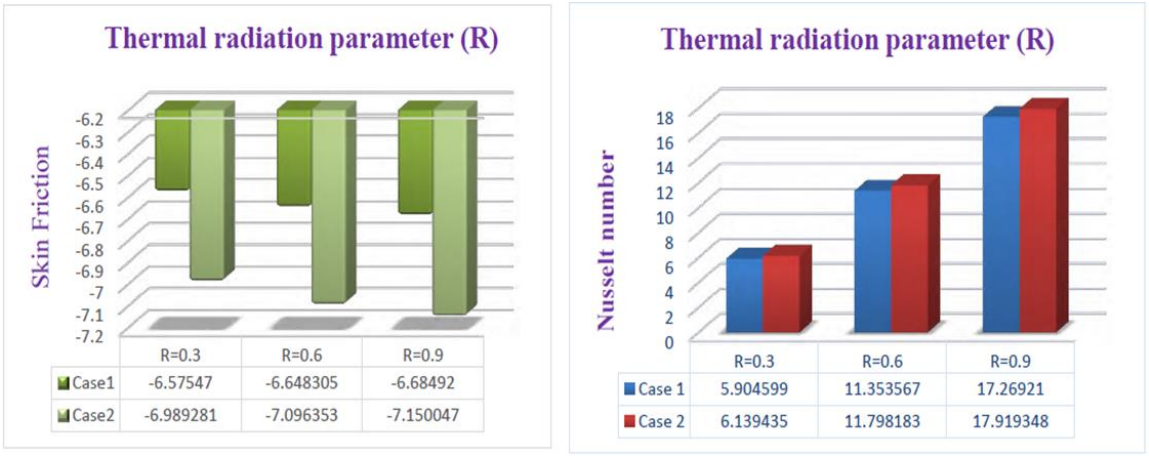

Figure 20(b). Depicts the bar graph of Thermal radiation parameter (R) with Nusselt number and skin friction for two different combination of ternary hybrid nanofluid.

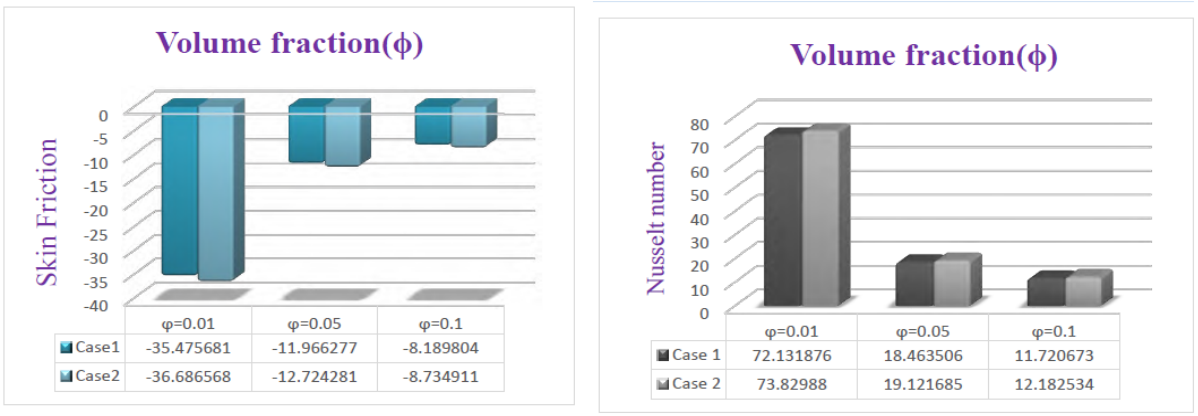

Figure 20(c). Depicts the bar graph of Volume fraction parameter (ϕ) with Nusselt number and skin friction for two different combination of ternary hybrid nanofluid.

Figure 20(d). Depicts the bar graph of Mixed convection parameter (λ) with Nusselt number and skin friction for two different combination of ternary hybrid nanofluid.

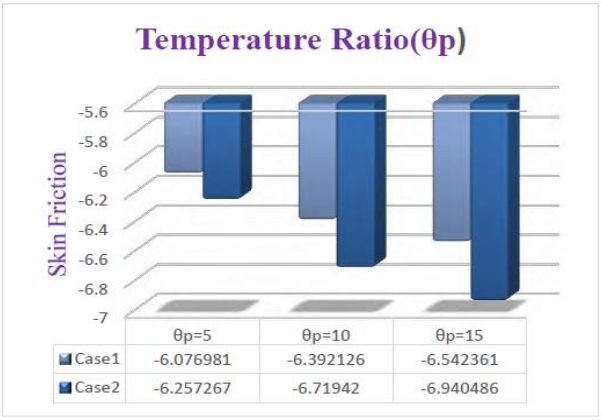

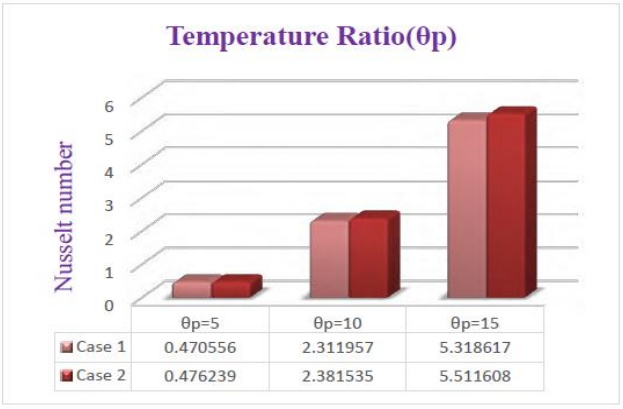

Figure 20(e). Depicts the bar graph of Temperature Ratio (θ_p) with Nusselt number and skin friction for two different combination of ternary hybrid nanofluid.

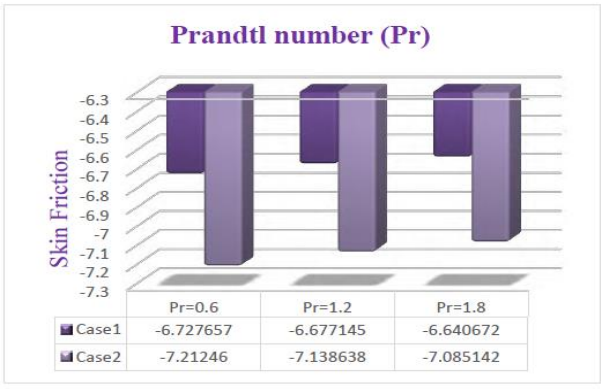

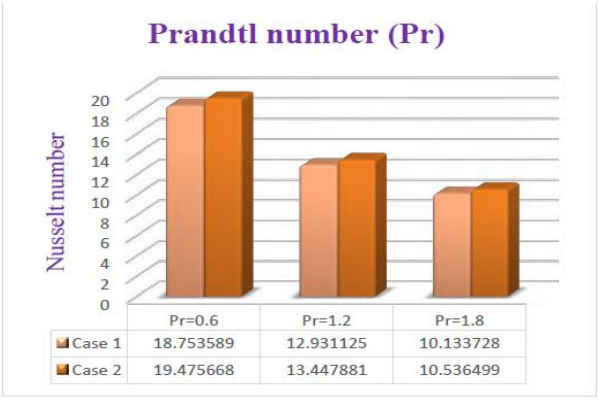

Figure 20(f). Depicts the bar graph of Prandtl number (Pr) with Nusselt number and skin friction for two different combination of ternary hybrid nanofluid.

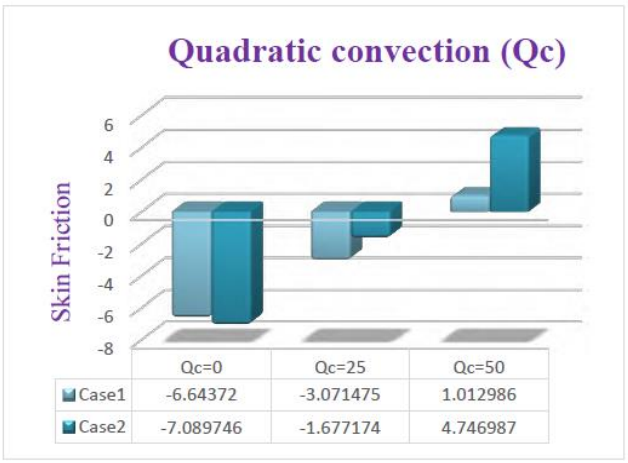

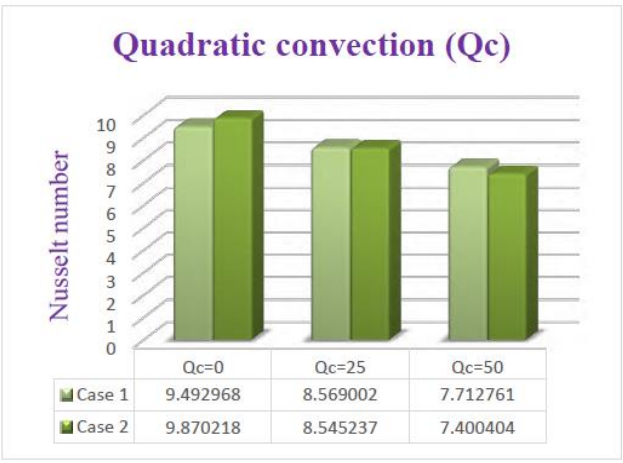

Figure 20(g). Depicts the bar graph of Quadratic convection (Q_c) with Nusselt number and skin friction for two different combination of ternary hybrid nanofluid.

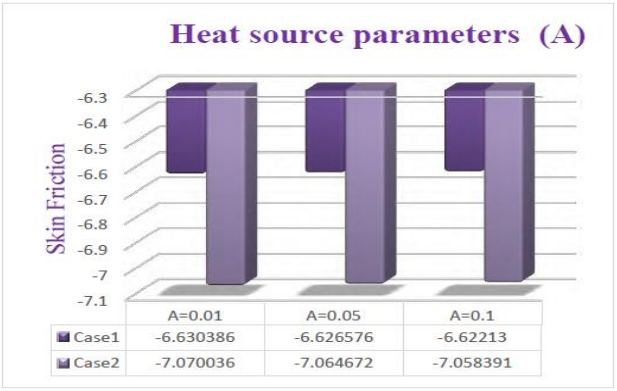

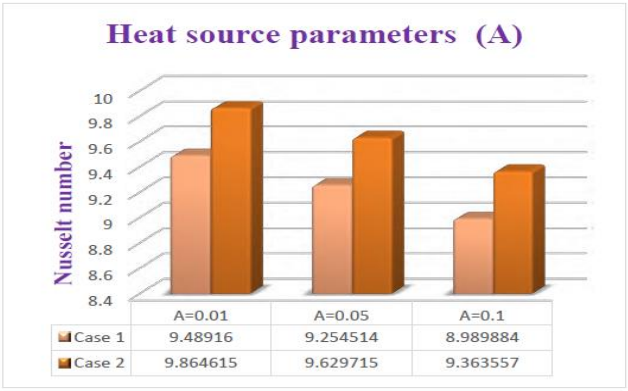

Figure 20(h). Depicts the bar graph of Heat source parameter (A) with Nusselt number and skin friction for two different combination of ternary hybrid nanofluid.

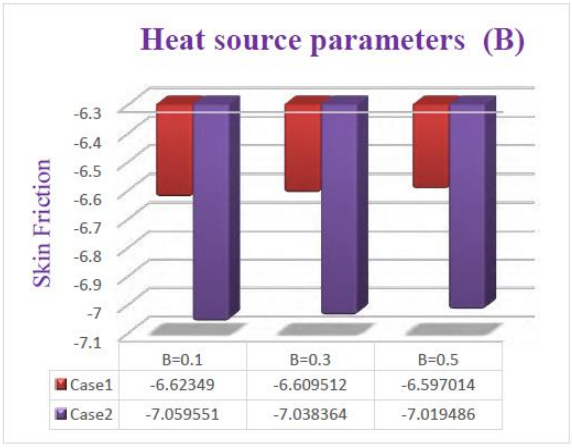

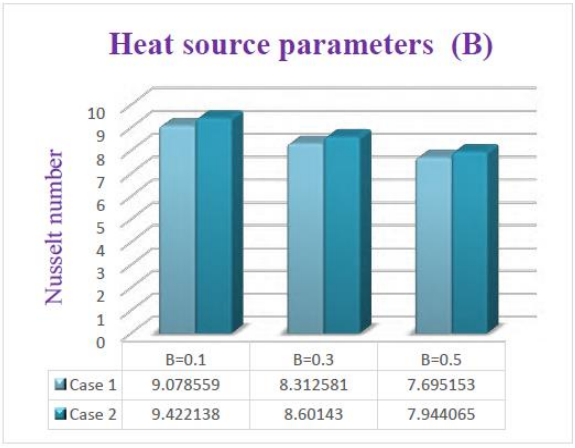

Figure 20(i). Depicts the bar graph of Heat source parameter (B) with Nusselt number and skin friction for two different combination of ternary hybrid nanofluid.

5. Conclusions

In recent years, fluid mixtures have become more and more important in various systems, including medicinal treatments, industry, experimental instrument design, aerosol particle processing, and naval academies. The Rosseland approximation on 3D flow characteristics is nonlinear, linear, and quadratic due to the presence of Fourier flux and Boussinesq second order thermal variation. Ternary hybrid nanoparticle densities and various shapes are included. The governing system that results is then tweaked, and a solution with two different mixture compositions is shown (Case-I and Case-II). Graphene (Cylindrical), Carbon nanotubes (Spherical), and aluminum oxide (Platelet) were considered in the first mixture, whereas copper (Cylindrical), copper oxide (Spherical), and silver oxide (Platelet) were studied in the second mixture. In comprehensive literature study it is observed that, many researchers claim that conventional fluids such as water, oil, ethylene glycol, glycerol etc. has comparatively lesser thermal properties compared with solid metals. Considering the enormous demand for energy and on other side diminishing world resources and environmental concerns has impelled the researchers towards the development of more efficient heat transfer fluids with upgraded

heat transfer rates. In recent days, fascinated by the applications/physical and chemical properties of nanoparticles researchers have initiated in exploring heat and flow properties of the colloidal mixture convectional fluid with three types of nanoparticles, known as ternary hybrid nanofluid. By considering this into view, investigated the slender surface flow characteristics in the presence of ternary nanoparticles. It is using MATLAB using bvp5c solver. The results are as follows:

1) Case-II ternary mixtures have a narrower temperature variation than Case-I ternary mixtures.
2) Compared to Case-1, Case-2 has a low skin friction coefficient.
3) The ternary hybrid nanofluid velocity increases as *n, R*, θ_p, Q_c, *A*, *B* and λ grow.
4) The ternary hybrid nanofluid velocity is decreases as *Pr* and φ grow.
5) The temperature of the ternary hybrid nanofluid rises for the values of *n, R*, φ, θ_p, *A and B* are estimated to be greater.
6) The ternary hybrid nanofluid temperature is a decreasing as of *Pr,* Q_c, and λ grow.

Data Availability

Data available on request from the authors.

Acknowledgements

This research received funding support from the NSRF via the Program Management Unit for Human Resources & Institutional Development, Research and Innovation, (grant number B05F650018).

Conflict of interest

The authors declare no conflicts of interest.

References

1. H. Yarmand, S. Gharehkhani, G. Ahmadi, S. F. S. Shirazi, S. Baradaran, E. Montazer, et al., Graphene nanoplatelets-silver hybrid nanofluids for enhanced heat transfer, *Energy Convers. Management*, **100** (2015), 419–428. https://doi.org/10.1016/j.enconman.2015.05.023
2. O. K. Koriko, K. S. Adegbie, I. L. Animasaun, M. A. Olotu, Numerical solutions of the partial differential equations for investigating the significance of partial slip due to lateral velocity and viscous dissipation: the case of blood-gold Carreau nanofluid and dusty fluid, *Numer. Methods Part. Differ. Equ.*, 2021. https://doi.org/10.1002/num.22754
3. Y. N. Jiang, X. M. Zhou, Y. Wang, Effects of nanoparticle shapes on heat and mass transfer of nanofluid thermocapillary convection around a gas bubble, *Microgravity Sci. Technol.*, **32** (2020), 167–177.
4. M. C. Arno, M. Inam, A. C. Weems, Z. Li, A. L. A. Binch, C. I. Platt, et al., Exploiting the role of nanoparticle shape in enhancing hydrogel adhesive and mechanical properties, *Nat. commun.*, **11** (2020), 1–9.

5. L. Th. Benos, E. G. Karvelas, I. E. Sarris, A theoretical model for the manetohydrodynamic natural convection of a CNT-water nanofluid incorporating a renovated Hamilton-Crosser model, *Int. J. Heat Mass Trans.*, **135** (2019), 548–560. https://doi.org/10.1016/j.ijheatmasstransfer.2019.01.148
6. H. Liu, I. L. Animasaun, N. A. Shah, O. K. Koriko, B. Mahanthesh, Further discussion on the significance of quartic autocatalysis on the dynamics of water conveying 47 nm alumina and 29 nm cupric nanoparticles, *Arab. J. Sci. Eng.*, **45** (2020), 5977–6004.
7. A. S. Sabu, A. Wakif, S. Areekara, A. Mathew, N. A. Shah, Significance of nanoparticles' shape and thermo-hydrodynamic slip constraints on MHD alumina-water nanoliquid flows over a rotating heated disk: the passive control approach, *Int. Commun. Heat Mass Trans.*, **129** (2021), 105711. https://doi.org/10.1016/j.icheatmasstransfer.2021.105711
8. Q. Lou, B. Ali, S. U. Rehman, D. Habib, S. Abdal, N. A. Shah, et al., Micropolar dusty fluid: Coriolis force effects on dynamics of MHD rotating fluid when Lorentz force is significant, *Mathematics*, **10** (2022), 2630. https://doi.org/10.3390/math10152630
9. M. Z. Ashraf, S. U. Rehman, S. Farid, A. K. Hussein, B. Ali, N. A. Shah, et al., Insight into significance of bioconvection on MHD tangent hyperbolic nanofluid flow of irregular thickness across a slender elastic surface, *Mathematics*, **10** (2022), 2592. https://doi.org/10.3390/math10152592
10. K. Vajravelu, Convection heat transfer at a stretching sheet with suction or blowing, *J. Math. Anal. Appl.*, **188** (1994), 1002–1011. https://doi.org/10.1006/jmaa.1994.1476
11. C-K. Chen, M-I. Char, Heat transfer of a continuous, stretching surface with suction or blowing, *J. Math. Anal. Appl.*, **135** (1988), 568–580. https://doi.org/10.1016/0022-247X(88)90172-2
12. R. N. Kumar, R. J. P. Gowda, A. M. Abusorrah, Y. M. Mahrous, N. H. Abu-Hamdeh, A. Issakhov, et al., Impact of magnetic dipole on ferromagnetic hybrid nanofluid flow over a stretching cylinder, *Phys. Scr.*, **96** (2021), 045215. https://doi.org/10.1088/1402-4896/abe324
13. B. Ali, I. Siddique, I. Khan, B. Masood, S. Hussain, Magnetic dipole and thermal radiation effects on hybrid base micropolar CNTs flow over a stretching sheet: finite element method approach, *Results Phys.*, **25** (2021), 104145. https://doi.org/10.1016/j.rinp.2021.104145
14. G. C. Rana, S. K. Kango, Effect of rotation on thermal instability of compressible Walters' (Model B′) fluid in porous medium, *J. Adv. Res. Appl. Math.*, **3** (2011), 44–57. https://doi.org/10.5373/jaram.815.030211
15. A. V. Kuznetsov, D. A. Nield, Thermal instability in a porous medium layer saturated by a nanofluid: Brinkman model, *Transp. Porous Media*, **81** (2010), 409–422.
16. L. J. Sheu, Linear stability of convection in a viscoelastic nanofluid layer, *Eng. Int. J. Mech. Mechatron. Eng.*, **5** (2011), 1970–1976.
17. L. L. Lee, Boundary layer over a thin needle, *Phys. Fluids*, **10** (1967), 820–822. https://doi.org/10.1063/1.1762194
18. J. L. S. Chen, Mixed convection flow about slender bodies of revolution, *ASME J. Heat Mass Trans.*, **109** (1987), 1033–1036. https://doi.org/10.1115/1.3248177
19. T. Fang, J. Zhang, Y. Zhong, Boundary layer flow over a stretching sheet with variable thickness, *Appl. Math. Comput.*, **218** (2012), 7241–7252. https://doi.org/10.1016/j.amc.2011.12.094
20. R. Jusoh, R. Nazar, I. Pop, Three-dimensional flow of a nanofluid over a permeable stretching/shrinking surface with velocity slip: A revised model, *Phys. Fluids*, **30** (2018), 033604. https://doi.org/10.1063/1.5021524

21. A. Jamaludin, R. Nazar, I. Pop, Three-dimensional magnetohydrodynamic mixed convection flow of nanofluids over a nonlinearly permeable stretching/shrinking sheet with velocity and thermal slip, *Appl. Sci.*, **8** (2018), 1128. https://doi.org/10.3390/app8071128
22. N. S. Khashi'ie, N. M. Arifin, R. Nazar, E. H. Hafidzuddin, N. Wahi, I. Pop, A stability analysis for magnetohydrodynamics stagnation point flow with zero nanoparticles flux condition and anisotropic slip, *Energies*, **12** (2019), 1268. https://doi.org/10.3390/en12071268
23. P. Rana, A. Kumar, G. Gupta, Impact of different arrangements of heated elliptical body, fins and differential heater in MHD convective transport phenomena of inclined cavity utilizing hybrid nanoliquid: Artificial neutral network prediction, *Int. Commun. Heat Mass Trans.*, **132** (2022), 105900. https://doi.org/10.1016/j.icheatmasstransfer.2022.105900
24. C. S. K. Raju, N. A. Ahammad, K. Sajjan, N. A. Shah, S-J. Yook, M. D. Kumar, Nonlinear movements of axisymmetric ternary hybrid nanofluids in a thermally radiated expanding or contracting permeable Darcy Walls with different shapes and densities: simple linear regression, *Int. Commun. Heat Mass Trans.*, **135** (2022), 106110. https://doi.org/10.1016/j.icheatmasstransfer.2022.106110
25. P. Rana, S. Gupta, G. Gupta, Unsteady nonlinear thermal convection flow of MWCNT-MgO/EG hybrid nanofluid in the stagnation-point region of a rotating sphere with quadratic thermal radiation: RSM for optimization, *Int. Commun. Heat Mass Trans.*, **134** (2022), 106025. https://doi.org/10.1016/j.icheatmasstransfer.2022.106025
26. N. A. Shah, A. Wakif, E. R. El-Zahar, T. Thumma, S.-J. Yook, Heat transfers thermodynamic activity of a second-grade ternary nanofluid flow over a vertical plate with Atangana-Baleanu time-fractional integral, *Alexandria Eng. J.*, **61** (2022), 10045–10053. https://doi.org/10.1016/j.aej.2022.03.048
27. R. Zhang, N. A. Ahammad, C. S. K. Raju, S. M. Upadhya, N. A. Shah, S-J. Yook, Quadratic and linear radiation impact on 3D convective hybrid nanofluid flow in a suspension of different temperature of waters: transpiration and fourier fluxes, *Int. Commun. Heat Mass Trans.*, **138** (2022), 106418. https://doi.org/10.1016/j.icheatmasstransfer.2022.106418
28. N. Acharya, Spectral quasi linearization simulation on the radiative nanofluid spraying over a permeable inclined spinning disk considering the existence of heat source/sink, *Appl. Math. Comput.*, **411** (2021), 126547. https://doi.org/10.1016/j.amc.2021.126547
29. P. Rana, W. Al-Kouz, B. Mahanthesh, J. Mackolil, Heat transfer of TiO2-EG nanoliquid with active and passive control of nanoparticles subject to nonlinear Boussinesq approximation, *Int. Commun. Heat Mass Trans.*, **126** (2021), 105443. https://doi.org/10.1016/j.icheatmasstransfer.2021.105443
30. T. Elnaqeeb, I. L. Animasaun, N. A. Shah, Ternary-hybrid nanofluids: significance of suction and dual-stretching on three-dimensional flow of water conveying nanoparticles with various shapes and densities, *Z. Naturforsch. A*, **76** (2021). https://doi.org/10.1515/zna-2020-0317
31. N. A. Shah, A. Wakif, E. R. El-Zahar, S. Ahmad, S-J Yook, Numerical simulation of a thermally enhanced EMHD flow of a heterogeneous micropolar mixture comprising (60%)-ethylene glycol (EG), (40%)-water (W), and copper oxide nanomaterials (CuO), *Case Study. Therm. Eng.*, **35** (2022), 102046. https://doi.org/10.1016/j.csite.2022.102046

32. M. S. Upadhya, C. S. K. Raju, Implementation of boundary value problems in using MATLAB®, In: *Micro and nanofluid convection with magnetic field effects for heat and mass transfer applications using MATLAB*, Elsevier, 2022, 169–238. https://doi.org/10.1016/B978-0-12-823140-1.00010-5
33. M. Khader, A. M. Megahed, Numerical solution for boundary layer flow due to a nonlinearly stretching sheet with variable thickness and slip velocity, *Eur. Phys. J. Plus*, **128** (2013), 100–108.

List of Symbols

n	Positive dimensional features parameter
(A, B)	Parameters of the heat source
q	Net heat flux, [W.m^{-2}]
C_{fx}	Coefficient of skin friction simplified
g	The acceleration of gravity, [m.s^{-2}]
Q_c	$Q_c = \frac{\beta_1}{\beta_0}(T_w - T_\infty)$ convective parameter (quadratic or nonlinear)
Gr_x	Local Grashof number
ρ_{bf}	The density of the base fluid (kg/m^3)
ρ_{hnf}	The ternary hybrid nanofluid's density (kg/m^3)
T_h	Temperature of the wall dimensions (K)
C_p	Specific heat, [J.kg^{-1}.K^{-1}]
T	A ternary hybrid nanofluid's dimensional temperature (K)
$(\rho c_p)_{hnf}$	The ternary hybrid nanofluid's heat capacity (kg/m^3)
T_∞	Fluid temperature at a distance from the wall (K)
$\mu_1 and\ \kappa_1$	A spherical nanofluid's viscosity and heat conductivity. (Ns/m^2 & W/m K)
$\mu_2 and\ \kappa_2$	A cylindrical nanofluid's viscosity and heat conductivity. (Ns/m^2 & W/m K)
$\mu_3 and\ \kappa_3$	A platelet nanofluid's viscosity and thermal conductivity (Ns/m^2 & W/m K)
u	The motion's dimensional velocity in the x-direction (m/s)
u_h	The motion along the x-axis is being stretched at a faster rate. (m/s)
v	The motion's dimensional velocity in the y-direction (m/s)
μ_{hnf}	The ternary hybrid nanofluid's dynamic viscosity (Ns/m^2)
ϕ_1	spherical nanoparticles volume/amount (m^3)
ϕ_2	cylindrical nanoparticles volume/amount (m^3)
ϕ_3	platelet nanoparticles volume/amount (m^3)
Nu	Nusselt number
ϕ_{hnf}	The ternary hybrid nanofluid's volume percent (m^3)
qr	Radiative heat flux, [W. m^{-2}]
$\theta p = \frac{T_h}{T_\infty}$	is the temperature ratio parameter.
Re	Reynold number
R	quadratic thermal radiation parameter, $R = \frac{4\sigma^* T_\infty^3}{kk^*}$
$u_h[x]$	velocity of stretch, [m. s^{-1}], $u_h[x] = [a + x]^n b$
$[x, y]$	Cartesian coordinates
P	Porosity parameter $= \frac{\mu_f}{(k_0 b \rho_f)}$
$[u, v]$	Components of velocity, [m/s]

Subscripts

r	Thermophysical qualities that are relative
s	Nanoparticles in solid form
∞	Condition of free-flow
f	a base liquid
w	Condition of the walls

Greek symbols

β	Casson parameter for hybrid nanofluids
β_T	Coefficient of thermal expansion, [K^{-1}]
φ	portion of a volume
μ	Dynamic viscosity, [Pa.s]
β_R	The absorption coefficient of Rossland, [m^{-1}]
σ	Electrical conductivity in a hybrid nanofluid, [$S.m^{-1}$]
σ_e	Constant of Stefan-Boltzmann, [$W.K^{-4}.m^{-2}$]
λ	Mixed convection parameter, $\lambda = \frac{Gr_x}{Re_x^2} = \left[\frac{c(\rho\beta_T)g}{b^2\rho_f}\right]$
ρ	Density, [$kg.m^{-3}$]
$[\rho C_P]$	Capacitance to heat, [$J.m^{-3}.K^{-1}$]
∇	Gradient vector, $\nabla = \left(\frac{\partial}{\partial x}, \frac{\partial}{\partial y}\right)$
$\gamma = \mu/\rho$	Kinematic viscosity, [$m^2.s^{-1}$]

AIMS Press

© 2023 the Author(s), licensee AIMS Press. This is an open access article distributed under the terms of the Creative Commons Attribution License (http://creativecommons.org/licenses/by/4.0)